Crystal Structure of Lumazine Synthase from *Mycobacterium tuberculosis* as a Target for Rational Drug Design: Binding Mode of a New Class of Purinetrione Inhibitors[†,‡]

Ekaterina Morgunova,[*,§] Winfried Meining,[§] Boris Illarionov,[||] Ilka Haase,[||] Guangyi Jin,[⊥] Adelbert Bacher,[||] Mark Cushman,[⊥] Markus Fischer,[||] and Rudolf Ladenstein[§]

Karolinska Institutet, NOVUM, Centre for Structural Biochemistry, S-14157 Huddinge, Sweden, Lehrstuhl für Organische Chemie und Biochemie, Technische Universität München, Lichtenbergstrasse 4, D-85747 Garching, Germany, and Department of Medicinal Chemistry and Molecular Pharmacology, School of Pharmacy and Pharmacal Sciences, Purdue University, West Lafayette, Indiana 47907

Received October 6, 2004; Revised Manuscript Received November 30, 2004

ABSTRACT: The enzymes involved in the biosynthesis of riboflavin represent attractive targets for the development of drugs against bacterial pathogens, because the inhibitors of these enzymes are not likely to interfere with enzymes of the mammalian metabolism. Lumazine synthase catalyzes the penultimate step in the riboflavin biosynthesis pathway. A number of substituted purinetrione compounds represent a new class of highly specific inhibitors of lumazine synthase from *Mycobacterium tuberculosis.* To develop potent antibiotics for the treatment of tuberculosis, we have determined the structure of lumazine synthase from *M. tuberculosis* in complex with two purinetrione inhibitors and have studied binding via isothermal titration calorimetry. The structures were determined by molecular replacement using lumazine synthase from *Saccharomyces cerevisiae* as a search model and refined at 2 and 2.3 Å resolution. The *R*-factors were 14.7 and 17.4%, respectively, and the R_{free} values were 19.3 and 26.3%, respectively. The enzyme was found to be a pentamer consisting of five subunits related by 5-fold local symmetry. The comparison of the active site architecture with the active site of previously determined lumazine synthase structures reveals a largely conserved topology with the exception of residues Gln141 and Glu136, which participate in different charge−charge interactions in the core space of the active site. The impact of structural changes in the active site on the altered binding and catalytic properties of the enzyme is discussed. Isothermal titration calorimetry measurements indicate highly specific binding of the purinetrione inhibitors to the *M. tuberculosis* enzyme with dissociation constants in micromolar range.

The prevalence of multiple-drug resistance in pathogenic microorganisms is at a steadily increasing rate becoming a major threat to human health around the world. An alarming example is the worldwide increasing multidrug resistance of *Mycobacterium tuberculosis*, a human pathogen, which is responsible for the death of millions of people every year. This disease has become such a public health threat that the World Health Organization has declared a public health emergency (*1*). The increasing incidence of antibiotic resistance has brought a new sense of urgency to the discovery and development of antibacterial drugs. The antibiotics, however, that are currently available attack only a handful of targets. As a consequence, the development of drugs that act on new targets is urgently needed.

Among the known strategies for designing new antibiotics, cofactor/coenzyme biosynthesis offers several important advantages for drug development. Most of the known microorganisms are strictly dependent on endogenous biosynthesis of cofactors, because they lack specific transport proteins and are therefore devoid of efficient uptake systems (*2*). The enzymes involved in cofactor biosynthesis pathways represent very specific targets for antibacterial growth inhibition, because these enzymes are usually not present in the human or animal host.

Recent genomic studies have suggested that the riboflavin biosynthesis pathway is essential for both *M. tuberculosis* and *Mycobacterium leprae* (*3*). The development of inhibitors against enzymes involved in riboflavin (vitamin B_2) biosynthesis opens a novel approach for the chemotherapy of mycobacterial infections. Notably, flavoenzymes, which use derivatives of riboflavin as their coenzyme, are indispensable for electron transport reactions in all cellular organisms. The enzyme targets of our interest are in the first line lumazine synthase and riboflavin synthase because those enzymes are well characterized in terms of structure and mechanism. It should be noted that compounds interfering with the biosynthesis of folic acid, a vitamin characterized by many

[†] This work was supported by the Swedish Research Council (Vetenskapsrådet) (Project 621-2001-3195).

[‡] The atomic coordinates and structure factors of MbtLS−TS-44 and MbtLS−TS-70 complexes have been deposited in the Protein Data Bank (entries 1W19 and 1W29, respectively).

* To whom correspondence should be addressed. E-mail: katja.morgunova@biosci.ki.se. Telephone: +46-8-6089290. Fax: +46-8-6089290.

[§] Karolinska Institutet.

[||] Technische Universität München.

[⊥] Purdue University.

10.1021/bi047848a CCC: $30.25
Published on Web 02/02/2005

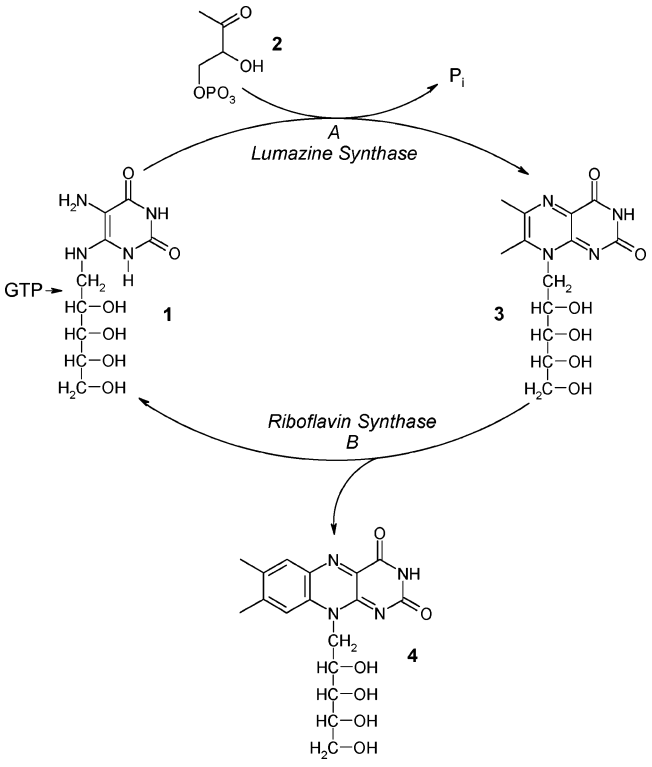

FIGURE 1: Biosynthesis of riboflavin: (**1**) 5-amino-6-ribitylamino-2,4(1*H*,3*H*)-pyrimidinedione, (**2**) 3,4-dihydroxy-2-butanone 4-phosphate, (**3**) 6,7-dimethyl-8-ribityllumazine, and (**4**) riboflavin.

structural and biosynthetic similarities with riboflavin, have a long and highly successful history as chemotherapeutic agents.

Lumazine synthase (LS)[1] and riboflavin synthase (RS) are two enzymes in the riboflavin biosynthesis pathway, catalyzing the formation of 6,7-dimethyl-8-(D-ribityl)lumazine and riboflavin, respectively. LS catalyzes the penultimate step of riboflavin biosynthesis, namely, the formation of 6,7-dimethyl-8-(D-ribityl)lumazine (**3**) from 3,4-dihydroxy-2-butanone 4-phosphate (**2**) and 5-amino-6-ribitylamino-2,4-(1*H*,3*H*)-pyrimidinedione (**1**) (Figure 1). Sequences of lumazine synthases from different organisms are 30−48% similar, and these enzymes exist in at least two oligomerization states (*4*, *5*). The enzymes from *Bacillus subtilis*, *Aquifex aeolicus*, *Escherichia coli*, and *Spinacia oleracea* form icosahedral capsids that consist of 60 identical subunits which can alternatively be described as dodecamers of pentamers. *B. subtilis* also forms a 1 MDa enzyme complex consisting of the LS capsid and three RS subunits enclosed in the central core. Several structures of empty capsids obtained by recombinant DNA technology have been determined in native form as well as in complex with inhibitors or substrate analogues (*6*−*10*). LS from *Saccharomyces cerevisiae*, *Schizosaccharomyces pombe*, *Brucella abortus*, *Magnaporthe grisea*, and *M. tuberculosis* assemble into stable homopentamers with a topology very similar to that of the pentameric modules in the icosahedral enzymes (*7*, *11*−*13*). In all LS structures, the topologically equivalent active sites are located at the interfaces between adjacent subunits in the pentamer. By comparing inhibitor binding data and considering structural constraints implied by the geometry of the active site, Zhang et al. (*9*) have suggested a catalytic mechanism which represents an extended and refined version of the mechanism proposed previously by Kis et al. (*14*). This mechanism consisted of the following steps: substrate binding, nucleophilic attack, formation of a Schiff base intermediate, phosphate elimination, and ring closure. The involvement of conserved key residues, i.e., Phe22, Arg127, and His88, and the Lys135/Glu138 couple of LS from *A. aeolicus* has been discussed on the basis of structural proximity and activity measurements on mutants of the highly homologous LS from *B. subtilis* (*9*).

Our work on the structure−function relationships of riboflavin biosynthetic enzymes as well as the potential of riboflavin biosynthesis as a target for antibacterial therapy has resulted in cooperative efforts concerning the design and synthesis of a number of inhibitors of LS and RS (*15*−*18*). At present, the kinetic inhibition constants and experimentally determined structures of complexes with several substrate analogue inhibitors, such as 5-nitroso-6-ribitylamino-2,4-(1*H*,3*H*)-pyrimidinedione (*7*, *9*), 5-nitro-6-ribitylamino-2,4-(1*H*,3*H*)-pyrimidinedione (*8*, *12*), and 5-[6-D-ribitylamino-2,4(1*H*,3*H*)-pyrimidinedione-5-yl]-1-pentylphosphonic acid (*9*, *13*), and also of the product analogues 6,7-dioxo-5*H*-8-ribitylaminolumazine and 3,7-hydroxy-8-ribitylumazine (*9*) are available. To obtain inhibitors of potential value as antibiotics, a series of ribitylpurinetriones bearing an alkyl phosphate group were recently designed and synthesized (*19*). These substances mimic a reaction intermediate of LS that binds to the active site. The compounds were found to be rather effective inhibitors for both *B. subtilis* LS and *E. coli* RS. Surprisingly, those purinetrione compounds showed the highest affinity for LS from *M. tuberculosis* (MbtLS) with kinetic inhibition constants in the nanomolar range (*19*). It is obvious that the inhibition effect of the ribitylpurinetrione phosphates is strongly dependent on the length of the aliphatic linker between the purinetrione ring system and the phosphate moiety.

To study in detail the binding of the potential MbtLS inhibitors with the future aim of developing antibacterial drugs directed against *Mycobacterium*, we have investigated two complexes of MbtLS with 3-(1,3,7,9-tetrahydro-9-D-ribityl-2,6,8-trioxopurin-7-yl)-1-propane 1-phosphate (TS-44) and 3-(1,3,7,9-tetrahydro-9-D-ribityl-2,6,8-trioxopurin-7-yl)-1-butane 1-phosphate (TS-70) by X-ray crystallography. In this paper, we present the results of the structure determination, the comparison of MbtLS with the previously known structures of lumazine synthases from different species, and the results of calorimetric binding studies.

MATERIALS AND METHODS

Molecular Biology and Enzymatic Methods. 5-Amino-6-ribitylamino-2,4(1*H*,3*H*)-pyrimidinedone and 6,7-dimethyl-8-ribityllumazine were synthesized by published procedures (*20*, *21*). Recombinant 3,4-dihydroxy-2-butanone 4-phosphate synthase of *E. coli* (*22*) was used for preparation of 3,4-dihydroxy-2-butanone 4-phosphate (*23*). Restriction enzymes were from New England Biolabs (Schwalbach, Germany). T4 DNA ligase was from Gibco BRL (Eggen-

[1] Abbreviations: MbtLS, *M. tuberculosis* lumazine synthase; LS, lumazine synthase; RS, riboflavin synthase; TS-44, 3-(1,3,7-trihydro-9-D-ribityl-2,6,8-purinetrion-7-yl)propane 1-phosphate; TS-70, 3-(1,3,7-trihydro-9-D-ribityl-2,6,8-purinetrion-7-yl)butane 1-phosphate; ITC, isothermal titration calorimetry.

Table 1: Bacterial Strains and Plasmids

	relevant characteristics	ref
E. coli strain		
XL1-Blue	recA1, endA1, gyrA96, thi-1, hsdR17, supE44, relA1, lac[F′, proAB, lacI^{q}ZΔM15, Tn10(tet^r)]	*26*
M15[pREP4]	lac, ara, gal, mtl, recA$^+$, uvr$^+$, Str^R, (pREP4: Kan^R, lacI)	*27*
expression plasmid		
pNCO113	expression vector	*27*
pNCO-MT-LS	expression plasmid for the overexpression of the gene encoding the lumazine synthase from *M. tuberculosis*	this study

Table 2: Oligonucleotides Used for the Construction of the Synthetic Gene Encoding the LS from *M. tuberculosis*

designation	sequence (5′ to 3′)
MT-LS-1	tgttgtagctcaagaactcgctcgtaatcatgatgctgttgtagcacttggtgttgtaatccgtggtc
MT-LS-2	gggttacagcatcgcaaacgtagtcgaaatgtggagtttgaccacggattacaacaccaagtgctacaac
MT-LS-3	ggtctcgatgaccctactgtagttcgtgttctcggtgcaatcgagattcctgttgtagctcaagaactcgctc
MT-LS-4	agcgataggcgtagaggaatccagagatacacggtcagaccttgggttacagcatcgcaaacgtagtc
MT-LS-5	gtgacgctctgctcgacggtgctcgtaaagttgctgccggttgtggtctcgatgaccctactgtagttc
MT-LS-6	ccagagcttgctcttcggtgttagtggtcagtacaccgttagcgataggcgtagaggaatccag
MT-LS-7	gttcgtctggctattgttgctagctcttggcatggtaaaatctgtgacgctctgctcgacggtgctcg
MT-LS-8	agcttgggcacctttgtcttcagcagacgtcgggagacccgcacgatccagagcttgctcttcggtgttag
MT-LS-9	atgcctgatctgccttctctcgatgcttctggtgttcgtctggctattgttgctagc
MT-LS-10	cacgcagggtcaatgcggtagcgagggctgcaacagtagcttgggcacctttgtcttcagc
MT-LS-11	ataatagaattcattaaagaggagaaattaactatgcctgatctgccttctctcgatg
MT-LS-12	tattatggatccttaagagtgagcacgcagctcacgcagggtcaatgcggtagcgag

stein, Germany). Taq Polymerase was from Finnzyme (Epsoo, Finland). DNA fragments were purified with the QIAquick PCR purification kit from Qiagen (Hilden, Germany). Oligonucleotides were custom-synthesized by MWG Biotech (Ebersberg, Germany).

Strains and Plasmids. Bacterial strains and plasmids used in this study are summarized in Table 1.

Restriction Enzyme Digestion of DNA. DNA was digested at 37 °C with restriction enzymes in reaction buffers specified by the supplier. The digested DNA was analyzed by horizontal electrophoresis in 0.8 to 3% agarose gels.

Enzyme Assay. The assay for lumazine synthase was performed as described previously (*24*).

Estimation of Protein Concentrations. Protein concentrations were estimated by the modified Bradford procedure reported by Read and Northcote (*25*).

Gene Synthesis. The overlapping oligonucleotides MT-LS-1 and MT-LS-2 were annealed, and a double-stranded DNA segment of 108 bp was obtained by DNA polymerase treatment. In a sequence of five PCR amplifications using that oligonucleotide as a template, the oligonucleotides listed in Table 2 were used pairwise (starting with MT-LS-3 and MT-LS-4) for the elongation of each prior amplificate. The final 510 bp amplificate was digested with *Eco*RI and *Bam*HI and ligated into the pNCO113 plasmid, which had been treated with the same restriction enzymes. The resulting plasmid designated pNCO-MT-LS was transformed into *E. coli* XL1-Blue cells by published procedures (*26*). Transformants were selected on LB agar plates supplemented with ampicillin (170 mg/L). The plasmid was re-isolated and transformed into *E. coli* M15[pREP4] cells (*27*) carrying the pREP4 repressor plasmid for the overexpression of the *lac* repressor protein. Kanamycin (15 mg/L) and ampicillin (170 mg/L) were added to secure the presence of both plasmids in the host strain.

SDS−Polyacrylamide Gel Electrophoresis. Sodium dodecyl sulfate−polyacrylamide gel electrophoresis was performed as described by Lämmli (*28*). Molecular weight standards were supplied by Sigma (Munich, Germany).

Analytical Ultracentrifugation. Experiments were performed with an Optima XL-A analytical ultracentrifuge from Beckman Instruments (Palo Alto, CA) equipped with absorbance optics. Aluminum double-sector cells equipped with quartz windows were used throughout. The partial specific volume was estimated from the amino acid composition (*29*). The protein concentration was monitored photometrically at 280 nm. For boundary sedimentation experiments, a solution containing 100 mM potassium phosphate (pH 7.0) and 2.3 mg/mL protein was centrifuged at 59 000 rpm and 20 °C. Sedimentation equilibrium experiments were performed with a solution containing 0.76 mg of protein per milliliter of 100 mM potassium phosphate (pH 7.0).

Purification. All purification steps were performed at 4 °C. Frozen cell mass (20 g) was thawed in 100 mL of 50 mM potassium phosphate (pH 7.0) containing 0.5 mM EDTA and 1.0 mM DTT (buffer A). The suspension was subjected to treatment with a French press and was then centrifuged. The supernatant was passed through a column of Q-Sepharose Fast Flow (2 cm × 18 cm) (Amersham Pharmacia Biotech, Freiburg, Germany) pre-equilibrated with buffer A (flow rate of 5 mL/min). The column was washed with 100 mL of buffer A and developed with a linear gradient of 0 to 1.0 M potassium chloride in buffer A (total volume of 700 mL). Lumazine synthase was eluted from 310 to 370 mL. The enzyme fraction was brought to a concentration of 1 M ammonium sulfate by slow addition of an equal volume of 2 M ammonium sulfate in buffer A. The solution was passed through a column of octyl-Sepharose 4 FF (1.5 cm × 12 cm) (Amersham Pharmacia Biotech) pre-equilibrated with 1 M ammonium sulfate in buffer A (flow rate of 5 mL/min). The column was washed with 40 mL of 1 M ammonium sulfate in buffer A and developed with a decreasing linear gradient of 1.0 to 0 M ammonium sulfate in buffer A (total volume of 300 mL). Fractions were combined, concentrated by ultrafiltration, and brought to a concentration of 1 M

ammonium sulfate in buffer A. The solution was passed through a column of phenyl-Sepharose FF 16/10 (Amersham Pharmacia Biotech) pre-equilibrated with 1 M ammonium sulfate in buffer A (flow rate of 3 mL/min). The column was washed with 100 mL of 1 M ammonium sulfate in buffer A and developed with a linear gradient of 1.0 to 0 M ammonium sulfate in buffer A (total volume of 100 mL). The enzyme was eluted from 75 to 82 mL. Fractions were combined, concentrated by ultrafiltration, and dialyzed against 100 mM potassium phosphate (pH 7.0) containing 0.5 mM EDTA and 1 mM DTT (buffer B). The solution was passed through a column of Superdex 200 HiPrep 26/10 (Amersham Pharmacia Biotech) which had been equilibrated with buffer B (flow rate of 3 mL/min). The column was developed with 360 mL of buffer B. The enzyme was eluted from 210 to 240 mL. Fractions were combined, concentrated by ultrafiltration, and transferred to 100 mM potassium phosphate (pH 7.1) containing 1 mM DTT (buffer C). According to SDS−PAGE, the protein sample contained less than 3% impurities.

Crystallization. MbtLS was crystallized in the presence of two inhibitor compounds 3-(1,3,7-trihydro-9-D-ribityl-2,6,8-purinetrione-7-yl)propane 1-phosphate (TS-44) and 3-(1,3,7-trihydro-9-D-ribityl-2,6,8-purinetrion-7-yl)butane 1-phosphate (TS-70). The crystals were obtained in sitting drops by the vapor diffusion technique with the following macroseeding procedure: 1 μL of protein solution (8 mg/mL) containing 50 mM potassium phosphate buffer (pH 7.0) and 1 mM DTT was mixed with 1 μL of a 4 mM inhibitor solution and 2 μL of the reservoir solution containing 100 mM ADA [*N*-(2-acetamido)-2-iminodiacetic acid] buffer at pH 6.4, 3.5 M potassium acetate, and 50 mM DTT. Small crystals appeared after 3−4 days and were used as seeds for macroseeding. Small single crystals were transferred to drops, containing 1 μL of protein solution and 1 μL of inhibitor solution, under the same conditions as in the original drops with 2 μL of a solution containing 100 mM ADA (pH 6.4), 50 mM DTT, 2 M potassium acetate, and 8−10% MPD. After equilibration of the drops for 2−3 weeks against the reservoir solution, the seeds grew to a size of 0.4 mm × 0.3 mm × 0.2 mm. Additional crystals appeared around the initial seed. All crystals were of sufficient quality for X-ray data collection.

Data Collection. Two X-ray intensity data sets for complexes of MbtLS with TS-44 and of MbtLS with TS-70 were collected on a MAR Research 345 Image plate detector system (DESY synchrotron beamline BW7B at the EMBL Outstation, Hamburg, Germany) at 100 K each from a single crystal using the reservoir solution as a cryoprotectant. Each data set was obtained at a wavelength of 0.85 Å and an oscillation range 1°. Space group and cell parameters were determined using the auto-indexing routine in DENZO (*30*) and have been checked with pseudoprecession images generated with Pattern (*31*). The X-ray data were evaluated and scaled with DENZO and SCALEPACK (*30*). Statistics of the data collection are given in Table 3.

Structure Determination. To determine the local symmetry in the asymmetric unit, self-rotation functions were calculated for both data sets using MOLREP (*32*) at 4 Å resolution with an integration radius of 30 Å. The search was carried out for χ angles of 180°, 120°, 90°, and 72° to check for the presence of 2-, 3-, 4-, and 5-fold axes, respectively. Ten peaks with a signal-to-noise ratio higher than 5σ were found for the χ angle of 180°, and only one peak with the same ratio was found at χ of 72°. No other peaks with a signal-to-noise ratio higher than 1.5σ were found in the list of self-rotation correlation maxima. Thus, the χ angles of the local symmetry axes supported the pentameric organization of the protein subunits.

Table 3: Data Collection and Refinement Statistics

	MbtLS−TS-44	MbtLS−TS-70
data collection		
resolution limit (Å)	2.0	2.3
no. of observed reflections	108126	71430
no. of unique reflections	52169	33902
highest-resolution shell (Å)	2.02−2.00	2.33−2.3
overall completeness (%)	99.4	98.0
completeness of the highest-resolution shell (%)	99.0	94.4
overall I/σ	10.26	8.02
last shell I/σ	3.8	5.6
overall R_{sym} (%)[a]	8.6	9.6
highest-resolution shell R_{sym} (%)	51.4	62.0
refinement		
no. of non-hydrogen protein atoms	5294	5283
no. of non-hydrogen inhibitor atoms	145 (29 × 5)	150 (30 × 5)
no. of non-hydrogen ion atoms	81	37
no. of solvent molecules	631	469
resolution range (Å)	19.92−2.0	25.5−2.3
overall R_{cryst} (%)[b]	14.7	17.4
R_{free} (%)[c]	19.3	26.8
Ramachandran plot		
most favorable regions (%)	92	93.7
allowed regions (%)	7.8	6.1
disallowed regions (%)	0.2	0.2
rms standard deviation		
bond lengths (Å)	0.12	0.020
bond angles (deg)	1.810	1.901
average *B*-factor (Å^2)	13.48	11.49

[a] $R_{sym} = \sum_i |I_i - \langle I_i \rangle| / \sum_i |\langle I_i \rangle|$, where I_i is the scaled intensity of the *i*th observation and $\langle I_i \rangle$ is the mean intensity for that reflection. [b] $R_{cryst} = \sum_{hkl} ||F_{obs}| - |F_{calc}|| / \sum_{hkl} |F_{obs}|$. [c] R_{free} is the cross-validation *R*-factor computed for the test set of 5% of the unique reflections.

To determine the position and orientation of the pentameric MbtLS molecule, the structure of a pentamer of *S. cerevisiae* LS (*13*) was used as a search model with all nonconserved residues replaced with alanine [Protein Data Bank (PDB) entry 1EJB].

The cross-rotation and translation search was conducted with AMORE as implemented in the CCP4 program package (*32*). A cross-rotation function was calculated in the resolution range of 15−4 Å with an integration sphere radius of 30 Å. From the list of correlation peaks with a possible orientation of the pentamer, the 10 highest peaks were used for the translation search, giving a correlation coefficient of 31.8%. The next highest peak had a correlation coefficient of 23.2%. After rigid body refinement, only one pentamer orientation was found with an *R*-factor of 53.4% and a correlation coefficient of 44.4%. Examination of the crystal packing with O (*33*) demonstrated reasonable crystallographic contacts of two pentamers around the crystallographic 2-fold axis. The asymmetric unit was found to contain only one pentamer with a corresponding Matthews coefficient of 2.4 Å^3/Da and 48% solvent content (*34*). The refined structure of the MbtLS−TS-44 complex was successfully used as a search model for the molecular replacement search of MbtLS in the data set of the MbtLS−TS-70 complex.

Refinement. The initial pentameric model was subjected to rigid body refinement conducted with CNS (*35*). Each of the five subunits was considered a rigid group. Two cycles of refinement, 250 steps each, with applied restrained noncrystallographic symmetry using data from 20 to 3 Å reduced the *R*-factors (R_{free}) from 51.8 (53.8%) to 51.3% (52.5%). The resulting coordinates were used to calculate an initial $2|F_o| - |F_c|$ electron density map. Solvent flattening, histogram matching, and 5-fold noncrystallographic averaging were applied to the initial electron density with DM as implemented in the CCP4 package (*32*) The mask covering one subunit was calculated with NCSMASK (*32*), and the noncrystallographic symmetry operators were improved after every cycle of averaging. This procedure dramatically improved the quality of the electron density map and allowed the building of almost all residues that had been replaced with alanine in the original model. The electron density for the inhibitor was clearly visible in the averaged map.

Further refinement using the TLS option and model building were carried out with REFMAC5 (*32*) and O (*33*), respectively. The progress of refinement was monitored by the R_{free} with 5% of the data set aside from the calculations. Five protein subunits and later five inhibitor molecules were assigned as separate TLS groups. The molecular model for the inhibitor was generated with O and the Monomer Library Sketcher (*32*). The dictionaries and libraries needed for the rebuilding and refinement were prepared by HIC-Up (*36*). The optimization of the geometric parameters was performed with CNS. After inclusion of the bound inhibitor and subsequent refinement of the protein models, the *R*-factor was reduced to 22.3% ($R_{free} = 26.4\%$). At this stage, solvent molecules were added with the help of ARP/WARP as implemented in the CCP4 package. In addition to 5 MbtLS subunits and 5 TS-44 molecules, a total of 631 water molecules, 13 K^+ ions, 6 DTT molecules, and 5 acetate ions were built into the $|F_o| - |F_c|$ map during several cycles of ARP/WARP, REFMAC5 refinement and manual rebuilding with O. The values of the final R_{cryst} and R_{free} are 14.7 and 19.3%, respectively. Details of the refinement statistics are presented in Table 3.

The structure of MbtLS in complex with inhibitor TS-70 was determined by molecular replacement with the MbtLS pentamer as a search model. Rigid body refinement, solvent flattening, averaging, and refinement were performed using a protocol similar to the one used for the MbtLS−TS-44 structure. The final model consists of 5 protein subunits, 5 inhibitor molecules, 469 water molecules, 13 K^+ ions, 4 acetate ions, and 1 DTT molecule. The final R_{cryst} value is 17.4%, and the R_{free} value is 26.3% at 2.3 Å resolution. The refinement statistics are presented in Table 3.

Purinetrione Inhibitors. 3-(1,3,7-Trihydro-9-D-ribityl-2,6,8-purinetrion-7-yl)propane 1-phosphate (TS-44) and 3-(1,3,7-trihydro-9-D-ribityl-2,6,8-purinetrion-7-yl)butane 1-phosphate (TS-70) were prepared as described elsewhere (*19*).

Isothermal Titration Calorimetry. Calorimetric measurements were carried out using a VP-ITC MicroCalorimeter (MicroCal, Inc., Northampton, MA). The reference cell was filled with water, and the instrument was calibrated using standard electrical pulses. All solutions were carefully degassed by stirring under vacuum before use. The binding isotherms of both ligands were measured by direct titration. A solution of MbtLS (0.002−0.06 mM) in 50 mM potassium phosphate buffer (pH 7.08) was titrated at 30 °C with 25 identical 3 μL injections at 2 min intervals. The syringe was filled with 1.6−2.2 mM inhibitor dissolved in the same buffer. The heat evolved after each injection was obtained from the integral of the calorimetric signal. The measured heat was obtained as a difference between the heat of binding and the corresponding heat of dilution. All data were evaluated with Microcal ORIGIN50 (Microcal Software). The association constants (K_a), binding enthalpy (ΔH), and stoichiometry (n) were obtained by fitting the data to standard equations for the binding using a model for sequential binding sites as implemented in Microcal ORIGIN50. The binding entropy (ΔS) and free energy (ΔG) of the binding were calculated from the basic thermodynamic equations ($\Delta G = -RT \ln K$) and the Gibbs−Helmholtz equation ($\Delta G = \Delta H - T\Delta S$).

RESULTS AND DISCUSSION

Cloning, Expression, and Purification. The hypothetical open reading frame (GenBank accession number E70902) of *M. tuberculosis*, which predicts a protein of 154 amino acid residues that are 46% identical to those of lumazine synthase of *A. aeolicus*, was amplified by PCR and was cloned into the pNCO113 expression vector. A recombinant *E. coli* strain carrying the resulting plasmid failed to produce significant amounts of the cognate protein. We therefore constructed a synthetic gene that was optimized for expression of the *M. tuberculosis* gene in *E. coli* by stepwise PCR elongation using six oligonucleotide pairs as primers. The synthetic DNA segment was cloned into the pNCO113 plasmid, and its sequence was verified by dideoxy termination sequencing. The sequence has been deposited in the GenBank (accession number AY730463).

A plasmid harboring the synthetic gene under the control of a T5 promoter and a *lac* operator directed the abundant synthesis of a protein with an approximate mass of 15.9 kDa in a recombinant *E. coli* strain. The recombinant protein was purified and appeared to be homogeneous as judged by sodium dodecyl sulfate−polyacrylamide gel electrophoresis.

The enzyme sediments at an apparent velocity of 4.8 S at 20 °C. Orthologous lumazine synthases with pentameric structure from the yeasts *Sc. pombe* and *S. cerevisiae* have been reported to sediment at similar rates of 5.0 and 5.5 S, respectively (*37*, *38*). Sedimentation equilibrium experiments indicated a molecular mass of 79 kDa using a model of an ideal monodisperse solution for calculation. The calculated subunit molecular mass of 15 901 Da implicates a pentamer mass of 79.5 kDa, in good agreement with the experimental data.

Crystallization, Data Collection, and Structure Determination. The first crystallization trials were performed with protein dissolved in Tris hydrochloride at pH 7.0 without any inhibitors. These attempts only yielded badly shaped crystals, which however could be used later as macro seeds for the cocrystallization of MbtLS with inhibitors. Using the macroseeding procedure described in Materials and Methods, well-shaped crystals with maximum dimensions of 0.4 mm × 0.3 mm × 0.2 mm were obtained 2−3 weeks after seeds had been added to the pre-equilibrated drop. The space group was determined to be monoclinic *C*2 for both complexes with slightly different cell dimensions: $a = 131.3$ Å, $b = 80.7$

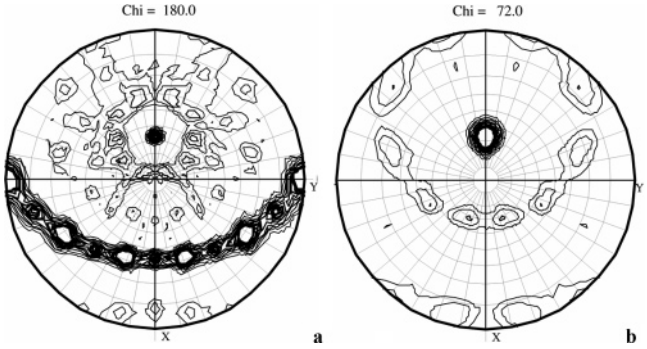

FIGURE 2: Stereogram plots of the self-rotation function $\chi = 180°$ (a) and $\chi = 72°$ (b) sections. The radius of integration was 30 Å, and the resolution limits were 20−4.0 Å. Polar angles are defined as implemented in the CCP4 package (*32*). Contour lines are drawn from 10.0σ in steps of 6σ. The plot was generated with MOLREP as implemented in the CCP4 program package.

Å, $c = 86.2$ Å, $\alpha = \gamma = 90°$, and $\beta = 120.3°$ for the MbtLS−TS-44 complex and $a = 131.4$ Å, $b = 80.8$ Å, $c = 86.0$ Å, $\alpha = \gamma = 90°$, and $\beta = 120.2°$ for the MbtLS−TS-70 complex. The asymmetric unit contained one pentamer.

Both structures were determined by molecular replacement at 2.0 and 2.3 Å resolution, respectively. The self-rotation function calculated with MOLREP revealed clear evidence for 5-fold particle symmetry. The $\chi = 72°$ section indicated a 5-fold axis lying in the $a-c$ plane at 58° inclination with respect to the a axis. The $\chi = 180°$ section indicated two sets of 2-fold, generated by the interaction of crystallographic and noncrystallographic symmetry operations. They are perpendicular to the 5-fold, one set of five peaks with a height of 37.8% and an angle of 36° between them as well as a second set of five peaks with a height of 17.9% and, as in the first set, with a 36° angle between the peaks. An angle of 18° was found between the neighboring peaks from both sets (Figure 2). This pattern of correlation peaks was well in line with the assumption of one pentamer in the asymmetric unit and showed that the 5-fold axes of the four pentamers in the unit cell are parallel. The correlation between the peaks in self- and cross-rotation functions confirmed the correct orientation of one pentamer in the asymmetric unit. Assuming one pentamer per asymmetric unit, the calculated Matthews coefficient appears to be 2.4 Å^3/Da with a respective solvent content of 48%.

MbtLS−TS-44 Complex. The cross-rotation and translation search performed in the MbtLS−TS-44 data set with the polyalanine model yielded a single dominant solution with good packing in the crystal lattice. The packing is characterized by face-to-face contact of two pentamers sharing a common 5-fold symmetry axis. This kind of contact is reminiscent of a similar packing interaction that was observed between pentamers in crystals of *S. cerevisiae* LS (*13*). The *R*-factor after rigid body refinement with noncrystallographic restraints and one monomer defined as a rigid body was 51.3% ($R_{free} = 52.5\%$). The initial electron density map calculated at that stage was well-defined for a major part of the main polypeptide chains of five subunits. Ten cycles of solvent flattening followed by 5-fold noncrystallographic averaging with DM improved the map dramatically and allowed the building of all side chains of the MbtLS sequence which had earlier been replaced with alanine residues. The electron density of the first 14 N-terminal residues was invisible for all five subunits and remained undefined throughout the refinement. The model was rebuilt and refined with isotropic *B*-factors during several cycles until the *R*-factor reached a value of 22.3% ($R_{free} = 26.4\%$). The electron density of the inhibitor was very well defined, and the inhibitor molecule was built after all side chains, for which there was interpretable density, had been introduced and refined. At the final stage of refinement, water molecules, potassium ions, acetate ions, and DTT molecules were incorporated into the model and refined. The final *R*-factor was 14.7%, and the final R_{free} was 19.3%.

The analysis of the final model with PROCHECK showed 92% of the residues in the most favored regions and 7.8% in the additional allowed regions of the Ramachandran plot. The final pentamer model corresponding to one asymmetric unit contained 5294 protein atoms, 5 inhibitor molecules, 631 water molecules, 13 potassium ions, 5 acetate ions, and 6 DTT molecules. Fourteen N-terminal residues remained untraceable in all five subunits. The electron density of residues Asp49, Asp50, Glu122, and Glu123 was rather diffuse with *B*-factors of up to 30 Å^3, indicating multiple conformations.

MbtLS−TS-70 Complex. The structure determination of the MbtLS−TS-70 complex was performed using a similar protocol with the MbtLS−TS-44 structure as a search model. The inhibitor molecule as well as potassium and acetate ions was removed from the model. The molecular replacement search yielded an unambiguous solution. After rigid body refinement, solvent flattening, and noncrystallographic 5-fold averaging, the electron density was of very good quality. Most side chains with the exception of the 15 N-terminal residues were clearly visible. The side chains for Asp49, Asp50, Glu122, and Glu123 again appeared to be rather diffused. The TS-70 molecules were clearly visible in each active site as well as 13 potassium ions at the same places as in the MbtLS−TS-44 complex. Because of a lower resolution, only 4 acetate ions, 1 DTT molecule, and 469 water molecules could be incorporated into the final electron density map. The refinement with individual isotropic *B*-factors reduced the *R*-factor to 17.3% and R_{free} to 26.8%. The conformations of 92% of the polypeptide bonds were found in the most favored region and 8% within the additionally allowed regions.

Structural Comparison. MbtLS as well as all other known LS orthologues belong to the family of α/β proteins with $\alpha/\beta/\alpha$ sandwich topology (Figure 3). The overall topology of this fold is $\beta 2 \alpha 1 \beta 3 \alpha 2 \beta 4 \alpha 3 \beta 5 \alpha 4 \alpha 5$, with $\alpha 2/\alpha 3$ and $\alpha 1/\alpha 4/\alpha 5$ forming the flanking helices and $\beta 2 \beta 3 \beta 4 \beta 5$ the central β-sheet. In icosahedral LSs (LSs from *B. subtilis*, *A. aeolicus*, and *Sp. oleracea*), the first eight N-terminal residues are known to build an extra fifth β-strand of the central β-sheet of the adjacent subunit, but they have a flexible conformation in the pentameric enzymes. In a LS sequence comparison, the presence of at least one proline among the first 10 residues in the pentameric enzymes and an absence of proline in this sequence region in the icosahedral oligomers were noted (*7*). It was proposed that the geometry of the Pro residue does not allow a proper alignment of the fifth β strand to the adjacent subunit and thus prevents LS containing a Pro in this area from forming icosahedral assemblies (Figure 4). The loop connecting $\alpha 1$ with $\beta 3$ is exposed to the bulk solvent. It is the shortest among all known structures and

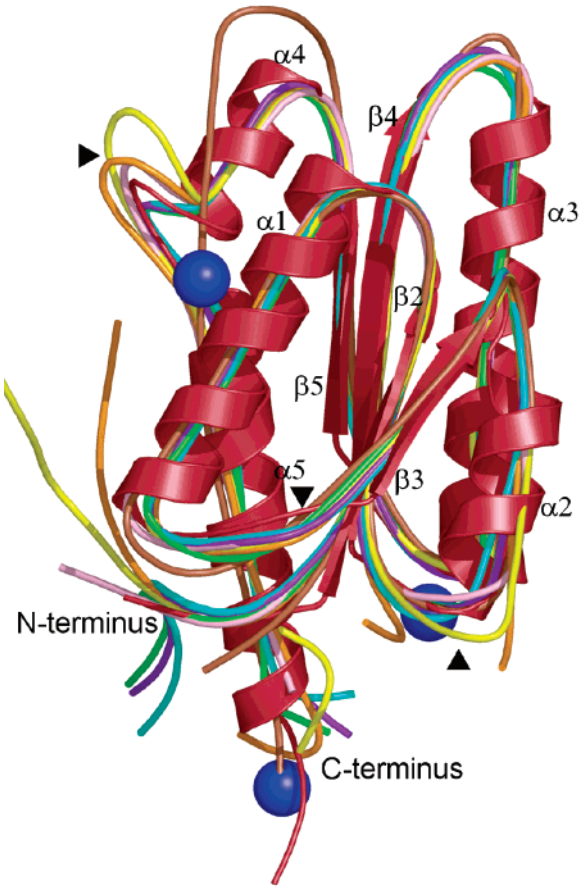

FIGURE 3: Secondary structure alignment of one subunit of lumazine synthase from *M. tuberculosis* (MbtLS) (red) with lumazine synthases from *S. pombe* (pink), *S. cerevisiae* (yellow), *B. abortus* (brown), *M. grisea* (orange), *B. subtilis* (violet), *A. aeolicus* (cyan), and *Sp. oleracea* (green). The secondary structure elements are assigned with respect to the MbtLS structure and labeled according to *B. subtilis* lumazine synthase (*6*, *8*). Blue spheres represent K^+ ions. Black arrowheads mark the loops, which show the structural differences. This figure was generated with PYMOL (*41*).

possesses almost no sequence similarity with other LS sequences. It is stabilized by formation of two hydrogen bonds between main chain carbonyl oxygens and amide nitrogens in the Ala43−Leu48 and Ala44−Gly47 pairs. The first H-bond is well conserved in some of the known structures (PDB entries 1RVV, 1KYV, 1C41, and 1HQK), but the second one is hitherto only observed in MbtLS.

The loop between α2 and β4 is also shortest in MbtLS in comparison to the other known LS structures. The sequence does not show any homology in this area, but insertions of different lengths are observed in all known LSs, the longest one consisting of 36 residues in *M. grisea* (*7*). In MbtLS, this loop participates in the face-to-face contact with the adjacent pentamer by forming the Arg71−Glu68′ salt bridge.

The β-hairpin loop connecting α4 and α5 is known as an essential region for the formation of the icosahedral capsid. In all LS structures which assemble to icosahedral particles, this loop comprises the rather conserved G(T/G)K(A/H)GN motif. In the pentameric enzymes, however, the loop shows different lengths with an insertion of up to four residues and adopts different conformations. In this loop region, the MbtLS sequence differs from sequences forming icosahedral LSs by four residues, whereas the structural alignment shows that this loop differs from the corresponding loop in the icosahedral ones by only two residues. In *B. abortus* LS, the insertion forms a part of a continuous helix with no multiple contacts with the neighboring pentamer, but it still prevents the isocahedral assembly (*11*). In this respect, *B. abortus* LS deviates from all other known pentameric LS structures. The conformation of the loop in MbtLS is stabilized by five hydrogen bonds formed between main and side chain atoms inside the loop. Its orientation is strictly fixed by three hydrogen bonds between main and side chain atoms with residue Asp127 from helix α4. The alignment of three MbtLS subunits with a trimer of the icosahedral *B. subtilis* LS revealed that even the short two-residue insertion is enough to produce a clash with the loop connecting strand β2 and helix α1 in the adjacent subunit. Interestingly, the four-residue addition in this loop in *A. aeolicus* LS resulted in the formation of large $T = 3$ icosahedral particles but not in the disassembly of $T = 1$ icosahedrons to pentamers (X. Zhang et al., unpublished results).

Thirteen peaks of strong spherical electron density over 5σ were found in the $|F_o| - |F_c|$ electron density map and were interpreted as potassium ions because of the high concentration of potassium acetate (3.5 M) used as a precipitating agent during the crystallization. Each subunit coordinates two K^+ ions. Every pair of subunits, connected by a local 2-fold axis, generated by the interaction of crystallographic and noncrystallographic symmetry operations, shares one K^+ ion, and two subunits connected by a crystallographic 2-fold axis share one K^+ ion, too (Figure 3). Both K^+ ions found inside the monomer exhibit a slightly distorted octahedral coordination provided by three or four main chain and side chain oxygen atoms and two or three water molecules, respectively, with an average distance of 2.85 Å. One potassium ion is found to make two contacts with the main chain oxygen atoms of Ala70 and His73 in the loop linking helix α2 and strand β4 and one contact with the side chain OG1 atom from Thr110 in the loop between helix α3 and strand β5. The other K^+ ion stabilizes the conformation of the loop that connects helices α4 and α5. It makes two contacts with main chain oxygen atoms of Ala129 and Gly130 and one contact with the carboxyl oxygen of Asp137. The fourth contact of this K^+ ion is formed with the main chain oxygen of Ala34 from helix α1. The potassium ion located on the 2-fold axis is liganded symmetrically by two main chain oxygens of each subunit with a distance of 3 Å from the metal ion and two water molecules in addition to the octahedral coordination.

Pentamer Assembly. MbtLS belongs to the class of pentameric LSs in contrast to the other icosahedral LSs. The pentameric nature of MbtLS was shown by analytical ultracentrifugation and confirmed by the structural investigation presented in this paper (Figure 5). The central left-handed twisted superhelix channel, with a length of 30 Å and a smallest diameter of 8.6 Å, is formed by the α3 helices arranged around the 5-fold axis. Hydrophilic residues Asp107, Arg103, and Asp95 and polar residues Tyr95 and Gln99 expose their side chains to the channel and participate in hydrogen bond network formation with water molecules. A salt bridge between Arg103 and Asp107 is stabilizing one of the entrances, while the opposite one is stabilized by hydrophobic residues Pro88 and Phe90 and polar residue Tyr92. In the crystal structure, the channel is filled with water

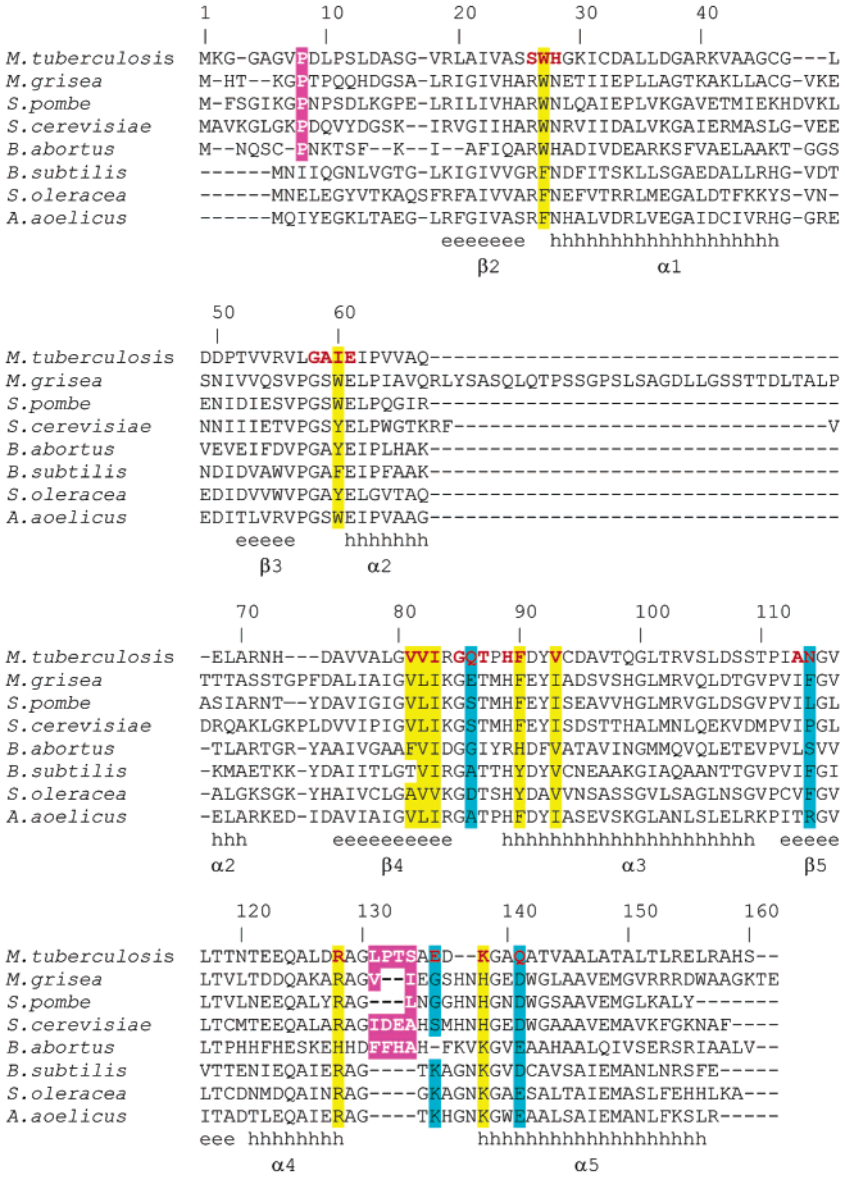

FIGURE 4: Sequence alignment of eight lumazine synthases with known structure. The residues involved in formation of the active site are colored red; putative residues, which may prevent icosahedral assembly, are colored magenta, and residues thought to be responsible for the specificity of lumazine synthase from *M. tuberculosis* (MbtLS) are colored cyan. Secondary structure elements are shown above the sequences as they are found in MbtLS. Sequence alignment was performed with CLUSTAL W (*42*).

molecules. The structural superposition of the α3 helices from eight known LS structures reveals a highly conserved arrangement with an rms deviation of 0.628 Å in *M. grisea* LS and 1.293 Å with *B. abortus* LS. However, sequence homology shows that none of the residues of α3 helices is conserved in all LSs. The alignment of the whole pentamers with the exception of 15 N-terminal residues indicates a tendency toward increasing structural differences between pentamers extending from the central channel to the peripheral parts. The rmsd between the remaining parts of the MbtLS pentamer and LSs from different organisms varies from 0.999 in *M. grisea* LS up to 1.402 in LS from *B. abortus*.

Inhibitor Binding Mode. The active site of all LSs known at present is located at the interface between two neighboring subunits in the pentameric assembly. The overall conformation of the MbtLS active site is very similar to those of the active sites of other LSs. All five substrate−product binding pockets within a pentamer have the same overall topology. It is formed by the residues from three β-loops connecting strands β2−β4 to helices α1−α3 (residues 26−28, 58−61, and 81−87, respectively) from one subunit as well as residues 128−141 from helices α4 and α5 and residue Asn114 from strand β5 of the neighboring subunit (Figure 6). There are in total 20 hydrogen bonds and 2 ionic contacts through which the TS-44 molecule is bound to the two subunits forming the active site: 7 contacts are made with one subunit, 4 made with the second one, and 11 contacts mediated by water molecules (Figure 6a,c). The heteroaromatic ring systems of both inhibitors are effectively packed in the hydrophobic part of the active site formed by Trp27, Ile60, Val81, Val82, Ile83, Phe90, and Val93 of one subunit. The purinetrione rings are located in a stacking position with the aromatic ring system of Trp27 3.5 and 4.5 Å from the side chains of Val83 and Val93, respectively, from the other sides of the cavity. The hydrophobic environment is highly conserved in all known LS active sites with respect to the equivalent substitutions of the hydrophobic residues; in

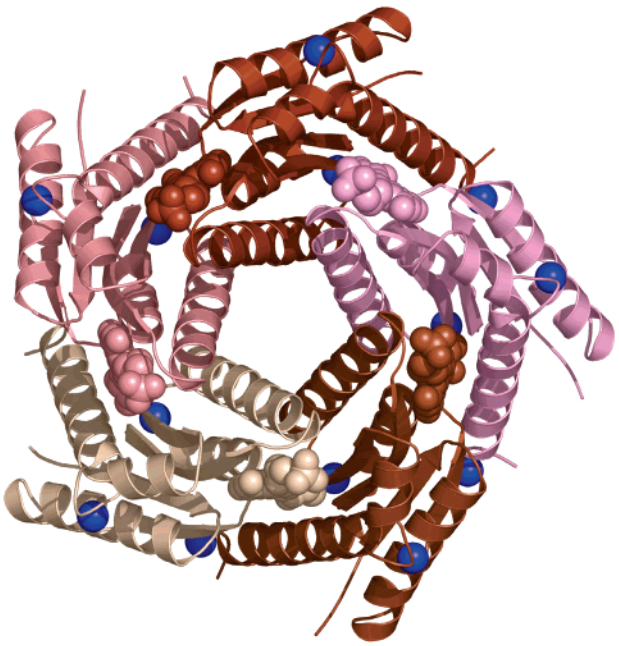

FIGURE 5: Pentameric assembly of lumazine synthase from *M. tuberculosis* viewed along the 5-fold noncrystallographic axis. The active sites located between subunits are occupied by 3-(1,3,7-trihydro-9-D-ribityl-2,6,8-purinetrion-7-yl)propane 1-phosphate (TS-44). Blue spheres represent potassium ions.

particular, Trp27 is often replaced with Phe and Val93 can be replaced with Ile. It is important to note that this cavity in MbtLS is lacking the offset stacking aromatic interaction observed in almost all known LSs between Trp57/Phe/Tyr and Phe113/Leu (*A. aeolicus* LS numbering) as a result of substitution by Ile60′ and Asn114′, respectively. The hydrophobic interaction of the purinetrione rings is supported by hydrogen bonds formed between the main chain O atom of Val81 and N3 from purinetrione rings, the main chain N atom of Ala59 and O2 of purinetrione, the main chain N atom of Val81 and the main chain O atom of Trp27 mediated by Wat25 with O2, and the NE2 atom of His28 and the main chain O atom of Ile83 with O4 mediated by Wat202. A schematic diagram of protein−inhibitor interactions is presented in Figure 6a,c. The carbonyl O6 of the purinetrione ring is fixed by a unique H-bond with the amide NZ atom of Lys138′ with a distance of 3.03 Å. This Lys is conserved in many LSs; however, in some LSs, it is replaced with His. Usually, this residue adopts a different conformation and is supposed to play some role in the phosphate transferring process during the catalytic reaction. The purinetrione compounds are the first of a series of rationally designed inhibitors, which make contact with the Lys138 side chain (*18*, *19*). The binding of the ribityl moiety of the purinetrione inhibitors is very similar to the binding of the ribityl chains of all previously known inhibitors. The ribityl chain is embedded in a surface depression formed by residues 56−62 from one subunit and one end of β5 (residues 113 and 114) of the adjacent subunit with several H-bonds to both subunits. The main chain N and O atoms of Asn114′ are hydrogen-bonded to O5′ and O4′, respectively, and the carboxyl oxygen atoms of Glu61 form hydrogen bonds with O3′ and O5′, respectively; O3′ forms a hydrogen bond to the OE1 atom of Glu61, and O2′ is H-bonded to the main chain N atom of Ile60. Those contacts are strictly conserved in all structurally investigated LSs.

The phosphate moiety occupies the putative position of 3,4-hydroxy-2-butanone 4-phosphate (**2**) (Figure 1), the second substrate of LS. Several contacts formed by the phosphate moiety of the novel inhibitors are strictly conserved among all known structures of LSs. O32 is H-bonded to the main chain N atom of Gln86 through Wat470, and O33 forms several contacts with the main chain N atom and the side chain OG1 atom of Thr87 and with the N atom of Gly85 and the O atom of Thr87, mediated by Wat19. O31 forms a H-bond with the NE atom of Arg128. Several contacts are mediated by water molecules: to OG1 of Thr87 through Wat386 and to OE1 and OE2 of Glu136′ and to NZ of Lys138′ through Wat259. Wat259 is also mediating the contact of O27 with Glu136′ and Lys138′.

The structural alignment of the two bound inhibitors reveals a slight difference in their binding modes that could be explained by the fact that the aliphatic chain of the TS-70 molecule bearing the phosphate group is one C−C bond longer than in TS-44. The conformation of this chain is slightly different in both inhibitors (Figure 6). The position of the phosphorus atom in TS-70 is shifted toward NH2 of Arg128′ by 1.1 Å on average in all five subunits, and CZ of Arg128′ is repositioned by 0.7 Å. The purinetrione rings occupy the same position as in the MbtLS−TS-44 complex, and the ribityl chain participates in the same contacts as in the MbtLS−TS-44 complex. The longer aliphatic linker of the phosphate moiety results in additional contacts, namely, O32 with the N atom of Gln86 and the NH atom of Arg128′ from the phosphate group part of the inhibitor and additional contacts of O2 and O4 with the OG atom of Ser25 and the NE2 atom of His28 from the purinetrione ring system (Figure 6b,d).

Isothermal Titration Calorimetry. Isothermal titration calorimetry (ITC) is the most direct method of measuring the heat that is generated or consumed upon formation of a ligand−macromolecule complex at a constant temperature. By least-squares fitting of the binding isotherms, we can derive the association constant (K_a), the binding enthalpy (ΔH), and the stoichiometry (n) of the process. Moreover, the entropy of the binding reaction (ΔS) and the free energy change (ΔG) are easily obtained from the relation $\Delta G = -RT \ln K_a = \Delta H - T\Delta S$.

To test purinetrione-based compounds for their inhibition potential, calorimetric measurements of the binding affinity were performed. Figure 7 shows representative calorimetric titration curves of MbtLS in 50 mM potassium phosphate buffer (pH 7.0) at 30 °C obtained with TS-44 and TS-70. The heat changes upon binding for each individual injection were plotted as a function of the molar inhibitor-to-protein ratio. The binding of both inhibitors is exothermic with negative changes in the binding enthalpy. To derive the thermodynamic parameters, the binding isotherms were initially fitted with a binding model assuming identical and independent binding sites. The fitting with this model, however, gave rather unsatisfactory results. Good fits of the isotherms could only be obtained by applying a model with five sequential binding sites. The analysis of the data revealed a molar binding stoichiometry (n) of 5 bound ligand molecules per pentamer which is in agreement with the X-ray structure presented in this paper. It appeared, however, that the five binding sites are not independent. They showed a weak cooperative behavior, which seems to be related to the

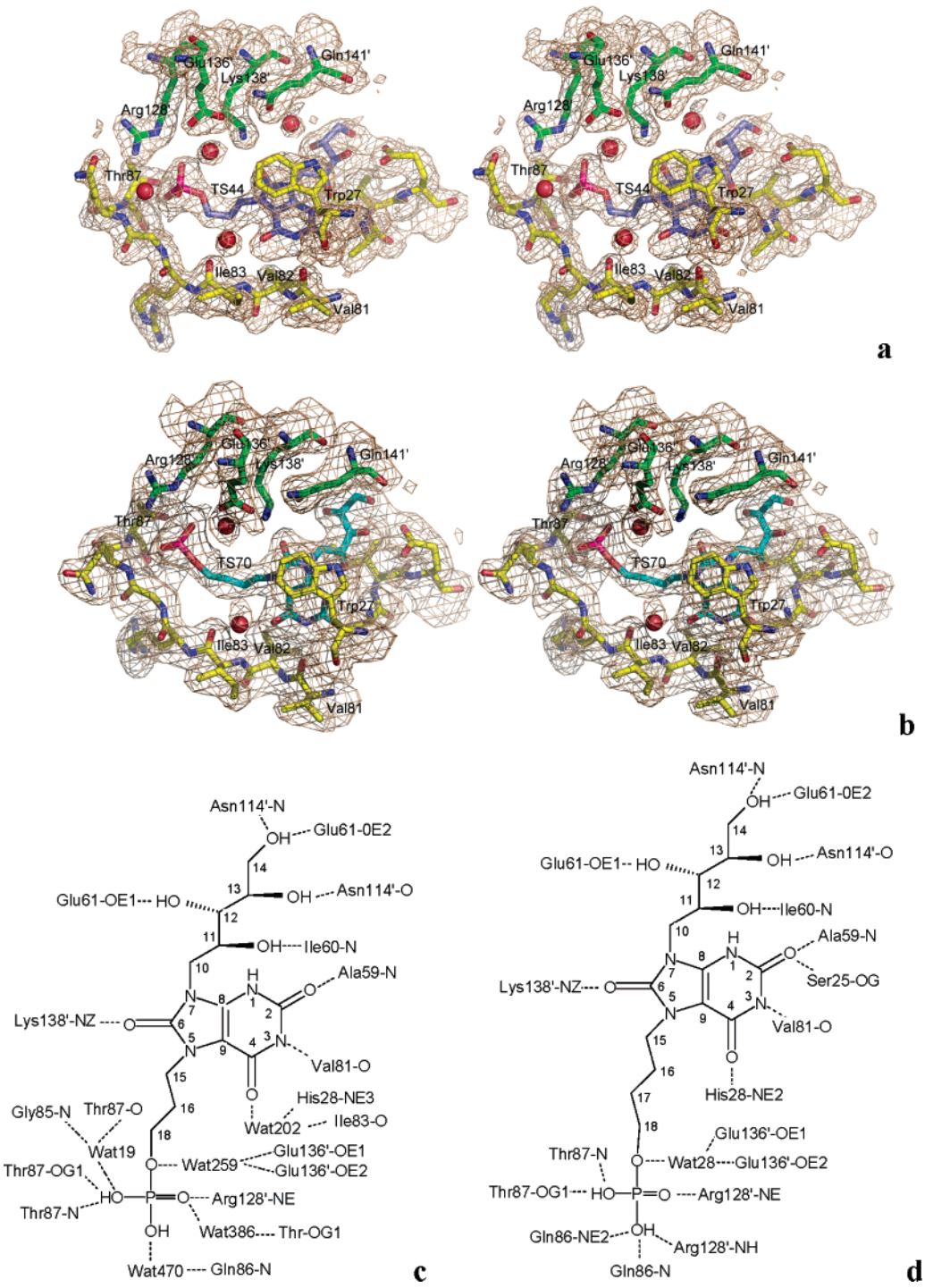

FIGURE 6: Stereodiagrams of the $2|F_o| - |F_c|$ electron density map ($\sigma = 2.5$) around the active site of *M. tuberculosis* lumazine synthase in complex with 3-(1,3,7-trihydro-9-D-ribityl-2,6,8-purinetrion-7-yl)propane 1-phosphate (TS-44, light blue) (a) and 3-(1,3,7-trihydro-9-D-ribityl-2,6,8-purinetrion-7-yl)butane 1-phosphate (TS-70, cyan) (b) and the respective schematic drawings of the interactions between the enzyme and the ligands (c and d). Red spheres represent water molecules. The carbon atoms of the residues of different subunits are colored green and yellow.

fact that an LS substrate−inhibitor binding site is formed by the interface created by two neighboring subunits of a pentamer. Both inhibitors showed a similar binding affinity for MbtLS with association constants $K_a = 4.768 \times 10^5 \pm 7.13 \times 10^4$ M^{-1} for the MbtLS−TS-44 complex and $K_a = 3.843 \times 10^5 \pm 8.738 \times 10^4$ M^{-1} for the MbtLS−TS-70 complex. Our observation is in agreement with the measurements of the inhibition constants of purinetrione inhibitors with LS from different species by a kinetic inhibition assay (*19*). Interestingly, similar titration calorimetry experiments with *B. subtilis* LS could not detect binding within the experimental limits in the case of both TS-44 and TS-70. For *B. subtilis* LS, the inhibition constants of both inhibitors are 100 times higher than for the *M. tuberculosis* enzyme as shown by the kinetic assay (*19*). The enthalpy of binding is characterized by favorable negative values of -12.72 ± 0.6 kcal/mol for the MbtLS−TS-44 complex and -13.83 ± 0.39 kcal/mol for the MbtLS−TS-70 complex. In both cases, the enthalpy and entropy terms have an opposite effect on the change in free energy (ΔG).

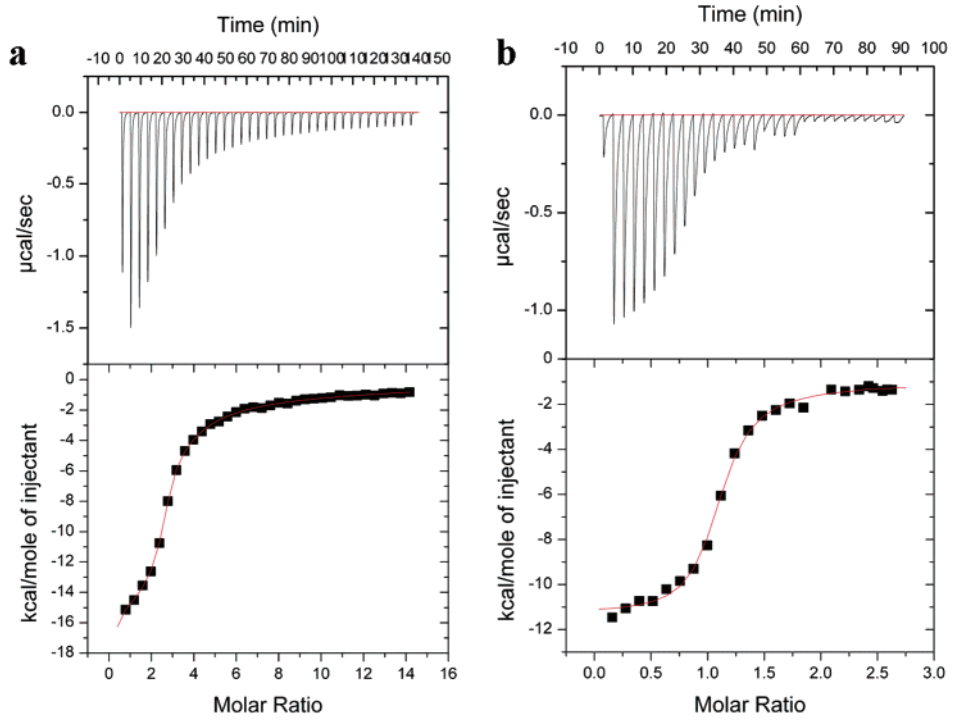

FIGURE 7: Typical isothermal titration calorimetry curves for lumazine synthase from *M. tuberculosis* titrated with 3-(1,3,7-trihydro-9-D-ribityl-2,6,8-purinetrion-7-yl)propane 1-phosphate (TS-44) (a) and 3-(1,3,7-trihydro-9-D-ribityl-2,6,8-purinetrion-7-yl)butane 1-phosphate (TS-70) (b). The top plots show titration data for the inhibitor binding. The bottom plots represent binding isotherms. The experiments were carried out as described in Materials and Methods.

The most favorable enthalpy change and most unfavorable entropy change were observed in titration studies with TS-44 and may result from a weakened ability of TS-44 to fill the active site properly due to, compared to TS-70, a shorter aliphatic linker. For both ligands, the enthalpic terms are larger than the entropic terms at 30 °C, indicating that the interactions between MbtLS and both compounds are enthalpically driven processes. However, because the interaction between MbtLS and TS-44 or TS-70 involves the removal of a phosphate ion which occupies the binding site of substrate **2** as well as several protonation and deprotonation events in the binding interface, a two-state (free → bound) model of the binding process is likely to be an oversimplification. Attempts to resolve the observed cooperativity of the binding process and the competitive removal of the phosphate ion by the inhibitor are in progress.

Implications for the Mechanism of Lumazine Formation. A landmark for the characterization of the enzymatic mechanism of LS was the identification of the second substrate, a four-carbon precursor of the pyrazine ring of 6,7-dimethyl-8-ribityllumazine (**3**) (Figure 1), which was identified by Volk and Bacher (*23*) as (3*S*)-3,4-dihydroxy-2-butanone 4-phosphate. A mechanism describing lumazine formation was suggested by Kis et al. (*14*) (Figure 8) and extended by Schramek et al. (*39*) and Haase et al. (*40*). The details of the catalytic mechanism have been investigated and discussed by Zhang et al. (*9*) on the basis of the structure of LS from *A. aeolicus* in free form as well as in complex with substrate−product analogues. According to the mechanism described by Zhang et al. (*9*) for *A. aeolicus* LS, residues Arg127′, Lys135′, and Glu138′ (*A. aeolicus* LS numbering, Figure 9b) are involved in positioning of the phosphate moiety of substrate 2. The side chain of Glu138′ can adopt different conformations in a cooperative manner

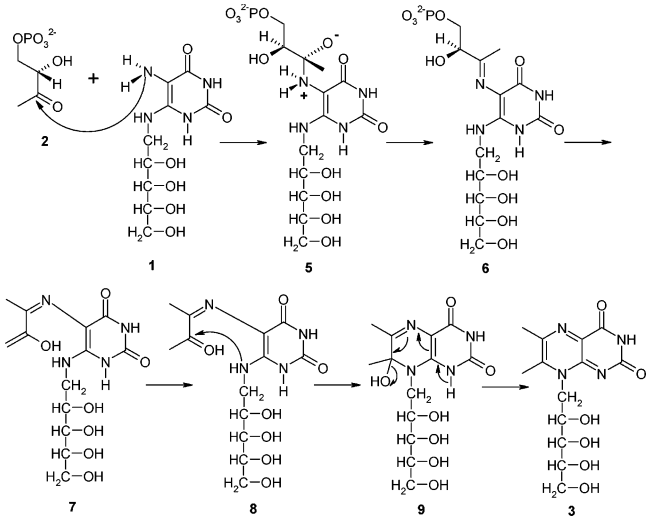

FIGURE 8: Hypothetical mechanism for the biosynthesis of lumazine suggested by Kis et al. (*14*).

together with Lys135′. A salt bridge between these residues is therefore conserved even after the change in their respective conformation. Since Lys135′ is in one of two observed conformations close to the phosphate moiety of bound substrate 2, it can build a salt bridge to the phosphate group. After conformational reordering of Lys135′ with retention of this salt bridge, the phosphate moiety could be reoriented and thus be removed from the original binding site. Enzyme kinetic studies of MbtLS performed by Cushman et al. (*19*) suggest tighter binding of the phosphate ion as well as a considerably decreased speed of the enzymatic reaction compared to the reaction speed of *B. subtilis* LS. The structure of MbtLS reveals differences in the active site, which could result in a slightly different kinetic behavior of the enzyme (Figure 9). Lys135′ and Glu138′ are in MbtLS

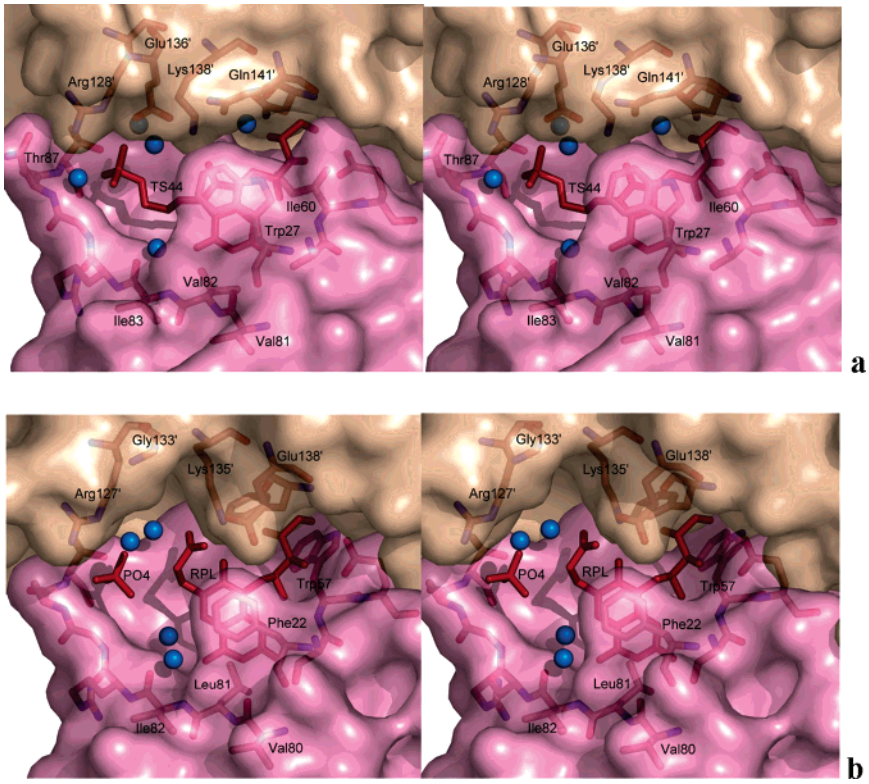

FIGURE 9: Stereoview of the surface representation of the active sites of lumazine synthase from *M. tuberculosis* in complex with the inhibitor 3-(1,3,7-trihydro-9-D-ribityl-2,6,8-purinetrion-7-yl)propane 1-phosphate (TS-44) (a) and *A. aeolicus* lumazine synthase in complex with 3-(7-hydroxy-8-ribityllumazin-6-yl)propionic acid (RPL) (PDB entry 1NQX) (b). The accessible surfaces were calculated with a water probe radius of 1.4 Å. Two adjacent subunits, constituting the active site, are shown in different colors (pink and wheat); the inhibitor molecules are colored red, and water molecules are colored light blue.

replaced with Lys138′ and Gln141′, respectively. A Gln residue in position 141 is unique for MbtLS among all LSs with known structure. A salt bridge between Lys138′ and Gln141′ is not possible anymore; however, a new negatively charged binding partner, Glu136′, is introduced into the active site as a replacement for the uncharged Gly133′. Glu136′ can probably form a salt bridge to Lys138′ and can therefore act as a negatively charged counterpart for Lys138′. The variation of its charge environment might hamper Lys138′ in its conformational variability and thus decrease the speed of the enzymatic reaction by reducing its ability to mediate a proper reorientation of the phosphate-bearing aliphatic chain that is needed to make the subsequent ring closure possible. The position and conformation of all other residues in the active site that were thought to take part in catalysis are conserved.

Conclusion. The structure of lumazine synthase from *M. tuberculosis* reveals new specific features of the active site that can be used as a structural basis for the development of specific inhibitors with an aim of designing new tuberculostatic agents. We have also demonstrated that compounds derived from purinetrione may serve as potential and specific inhibitors for MbtLS. Our future plans will include in vivo tests of the inhibitors described in this paper.

ACKNOWLEDGMENT

We thank Xiaofeng Zhang for technical assistance in the preparation of the manuscript. We gratefully acknowledge the access to synchrotron radiation facilities at the EMBL Outstation and thank the staff for help at the beamline.

REFERENCES

1. Nakajima, H. (1993) Tuberculosis: a global emergency, *World Health 46*, 3.
2. Dahl, S. G., Ingebrigt, S., and Westrheim, R. A. (2004) Structure and Models of Transporter Proteins, *J. Pharmacol. Exp. Ther. 309*, 853−860.
3. Cole, T. S., Eiglmeier, K., Parkhill, J., James, K. D., Thomson, N. R., Wheeler, P. R., Honore, N., Garnier, T., Churcher, C., Harris, D., Mungall, K., Basham, D., Brown, D., Chillingworth, T., Connor, R., Davies, R. M., Devlin, K., Duthoy, S., Feltwell, T., Fraser, A., Hamlin, N., Holroyd, S., Jagels, K., Lacroix, C., Maclean, J., Moule, S., Murphy, L., Oliver, K., Quail, M. A., Rajandream, M.-A., Rutherford, K. M., Rutter, S., Seeger, K., Simmonds, M., Skelton, J., Squares, R., Squares, S., Stevens, K., Taylor, K., Whitehead, S., Woodward, J. R., and Barrel, B.G. (2001) Massive gene decay in the leprosy bacillus, *Nature 409*, 1007−1011.
4. Bacher, A., Ludwig, H. C., Schnepple, H., and Ben-Shaul, Y. (1986) Heavy riboflavin synthase from *Bacillus subtilis*. Quaternary structure and reaggregation, *J. Mol. Biol. 187*, 75−86.
5. Zylberman, V., Craig, P. O., Klinke, S., Braden, B. C., Cauerhff, A., and Goldbaum, F. A. (2004) High order quaternary arrangement confers increased structural stability to *Brucella spp.* lumazine synthase, *J. Biol. Chem. 279*, 8093−8101.
6. Ladenstein, R., Schneider, M., Huber, R., Bartunik, H. D., Wilson, K., Schott, K., and Bacher, A. (1988) Heavy riboflavin synthase from *Bacillus subtilis*. Crystal structure analysis of the icosahedral β_{60} capsid at 3.3 Å resolution, *J. Mol. Biol. 203*, 1045−1070.
7. Persson, K., Schneider, G., Jordan, D. B., Viitanen, P. V., and Sandalova, T. (1999) Crystal structure analysis of a pentameric fungal and an icosahedral plant lumazine synthase reveals the structural basis for differences in assembly, *Protein Sci. 8*, 2355−2365.
8. Ritsert, K., Huber, R., Turk, D., Ladenstein, R., Schmidt-Bäse, K., and Bacher, A. (1995) Studies on the lumazine synthase/riboflavin synthase complex of *Bacillus subtilis*: Crystal structure

analysis of reconstituted, icosahedral β-subunit capsids with bound substrate analogue inhibitor at 2.4 Å resolution, *J. Mol. Biol. 253*, 151−167.
9. Zhang, X., Meining, W., Cushman, M., Haase, I., Fischer, M., Bacher, A., and Ladenstein, R. (2003) A structure-based model of the reaction catalyzed by lumazine synthase from *Aquifex aeolicus*, *J. Mol. Biol. 328*, 167−182.
10. Zhang, X., Meining, W., Fischer, M., Bacher, A., and Ladenstein, R. (2001) X-ray structure analysis and crystallographic refinement of lumazine synthase from the hyperthermophile *Aquifex aeolicus* at 1.6 Å resolution: Determinants of thermostability revealed from structural comparisons, *J. Mol. Biol. 306*, 1099−1114.
11. Braden, B. C., Velikovsky, C. A., Cauerhff, A. A., Polikarpov, I., and Goldbaum, F. A. (2000) Divergence in macromolecular assembly: X-ray crystallographic structure analysis of lumazine synthase from *Brucella abortus*, *J. Mol. Biol. 297*, 1031−1036.
12. Gerhardt, S., Haase, I., Steinbacher, S., Kaiser, J. T., Cushman, M., Bacher, A., Huber, R., and Fischer, M. (2002) The Structural Basis of Riboflavin Binding to *Schizosaccharomyces pombe* 6,7-Dimethyl-8-ribityllumazine Synthase, *J. Mol. Biol. 318*, 1317−1329.
13. Meining, W., Mörtl, S., Fischer, M., Cushman, M., Bacher, A., and Ladenstein, R. (2000) The atomic structure of pentameric lumazine synthase from *Saccharomyces cerevisiae* at 1.85 Å resolution reveals the binding mode of a phosphonate intermediate analogue, *J. Mol. Biol. 299*, 181−197.
14. Kis, K., Volk, R., and Bacher, A. (1995) Biosynthesis of riboflavin. Studies on the reaction mechanism of 6,7-dimethyl-8-ribityllumazine synthase, *Biochemistry 34*, 2883−2892.
15. Cushman, M., Mihalic, J. T., Kis, K., and Bacher, A. (1999) Design and synthesis of 6-(6-D-ribitylamino-2,4-dihydroxypyrimidin-5-yl)-1-hexyl phosphonic acid, a potent inhibitor of lumazine synthase, *Bioorg. Med. Chem. Lett. 9*, 39−42.
16. Cushman, M., Mihalic, J. T., Kis, K., and Bacher, A. (1999) Design, synthesis, and biological evaluation of homologous phosphonic acids and sulfonic acids as inhibitors of lumazine synthase, *J. Org. Chem. 64*, 3838−3845.
17. Cushman, M., Yang, D., Gerhardt, S., Huber, R., Fischer, M., Kis, K., and Bacher, A. (2002) Design, synthesis, and evaluation of 6-carboxyalkyl and 6-phosphonoxyalkyl derivatives of 7-oxo-8-ribitylaminolumazines as inhibitors of riboflavin synthase and lumazine synthase, *J. Org. Chem. 67*, 5807−5816.
18. Cushman, M., Yang, D., Kis, K., and Bacher, A. (2001) Design, synthesis, and evaluation of 9-D-ribityl-1,3,7-trihydro-2,6,8-purinetrione, a potent inhibitor of riboflavin synthase and lumazine synthase, *J. Org. Chem. 66*, 8320−8327.
19. Cushman, M., Sambaiah, T., Jin, G., Illarionov, B., Fischer, M., and Bacher, A. (2004) Design, synthesis, and evaluation of 9-D-ribitylamino-1,3,7,9-tetrahydro-2,6,8-purinetriones bearing alkyl phosphate and α,α-difluorophosphonate substituents as inhibitors of tiboflavin synthase and lumazine synthase, *J. Org. Chem. 69*, 601−612.
20. Sedlmaier, H., Müller, F., Keller, P. J., and Bacher, A. (1987) Enzymatic synthesis of riboflavin and FMN specifically labeled with ^{13}C in the xylene ring, *Z. Naturforsch. C42*, 425−429.
21. Vervoort, J., Muller, F., Mayhew, S. G., Berg, W. A. v. d., Moonen, C. T., and Bacher, A. (1986) A comparative carbon-13, nitrogen-15, and phosphorus-31 nuclear magnetic resonance study on the flavodoxins from Clostridium MP, Megasphaera elsdenii, and *Azotobacter vinelandii*, *Biochemistry 25*, 6789−6799.
22. Richter, G., Volk, R., Krieger, C., Lahm, H. W., Röthlisberger, U., and Bacher, A. (1992) Biosynthesis of riboflavin: Cloning, sequencing, and expression of the gene coding for 3,4-dihydroxy-2-butanone 4-phosphate synthase of *Escherichia coli*, *J. Bacteriol. 174*, 4050−4056.
23. Volk, R., and Bacher, A. (1990) Studies on the 4-carbon precursor in the biosynthesis of riboflavin. Purification and properties of L-3,4-dihydroxy-2-butanone-4-phosphate synthase, *J. Biol. Chem. 265*, 19479−19485.
24. Kis, K., and Bacher, A. (1995) Substrate channeling in the lumazine synthase/riboflavin synthase complex of *Bacillus subtilis*, *J. Biol. Chem. 270*, 16788−16795.
25. Read, S. M., and Northcote, D. H. (1981) Minimization of variation in the response to different proteins of the Coomassie blue G dye-binding assay for protein, *Anal. Biochem. 116*, 53−64.
26. Bullock, W. O., Fernandez, J. M., and Shout, J. M. (1987) XL1-blue: A high efficiency plasmid transforming recA *Escherichia coli* strain with β-galactosidase selection, *BioTechniques 5*, 376−380.
27. Stüber, D., Matile, H., and Garotta, G. (1990) in *Immunological Methods* (Lefkovits, I., and Pernis, B., Eds.) pp 121−152, Academic Press, New York.
28. Lämmli, U. K. (1970) Cleavage of structural proteins during the assembly of the head of bacteriophage T4, *Nature 227*, 680−685.
29. Laue, T. M., Shah, B. D., Ridgeway, T. M., and Pelletier, S. L. (1992) *Computer-aided interpretation of analytical sedimentation data for proteins*, Royal Society of Chemistry, Cambridge, U.K.
30. Otwinowski, Z., and Minor, W. (1997) Processing of X-ray Diffraction Data Collected in Oscillation Mode, *Methods Enzymol. 276*, 307−326.
31. Lu, G. (1999) PATTERN: A precession simulating program for displaying reflection data of reciprocal space, *J. Appl. Crystallogr. 32*, 375−376.
32. Collaborative Computational Project No. 4 (1994) The CCP4 Suite: Programs for Protein Crystallography, *Acta Crystallogr. D50*, 760−763.
33. Jones, A. T., Zou, J. Y., Cowtan, J. Y., and Kjeldgaard, M. (1991) Improved methods for building protein models in electron density maps and the location of errors in the model, *Acta Crystallogr. A47*, 110−119.
34. Matthews, B. W. (1968) Solvent content of protein crystals, *J. Mol. Biol. 33*, 491−497.
35. Brünger, A. T., Adams, P. D., Clore, G. M., DeLano, W. L., Gros, P., Grosse-Kunstleve, R. W., Jiang, J.-S., Kuszewski, J., Nilges, M., Pannu, N. S., Read, R. J., Rice, L. M., Simonson, T., and Warren, G. L. (1998) Crystallography & NMR System: A New Software Suite for Macromolecular Structure Determination, *Acta Crystallogr. D54*, 905−921.
36. Kleywegt, G. J., and Jones, T. A. (1998) Databases in protein crystallography, *Acta Crystallogr. D54*, 1119−1131.
37. Bacher, A., Fischer, M., Kis, K., Kugelbrey, K., Mörtl, S., Scheuring, J., Weinkauf, S., Eberhardt, S., Schmidt-Bäse, K., Huber, R., Ritsert, K., Cushman, M., and Ladenstein, R. (1996) Biosynthesis of riboflavin: Structure and mechanism of lumazine synthase, *Biochem. Soc. Trans. 24*, 89−94.
38. Braun, N., Meining, W., Hars, U., Fischer, M., Ladenstein, R., Huber, R., Bacher, A., Weinkauf, S., and Bachmann, L. (2002) Formation of metal nanoclusters on specific surface sites of protein molecules, *J. Mol. Biol. 321*, 341−353.
39. Schramek, N., Haase, I., Fischer, M., and Bacher, A. (2003) Biosynthesis of riboflavin. Single turnover kinetic analysis of 6,7-dimethyl-8-ribityllumazine synthase, *J. Am. Chem. Soc. 125*, 4460−4466.
40. Haase, I., Fischer, M., Bacher, A., and Schramek, N. (2003) Temperature-dependent presteady-state kinetics of lumazine synthase from the hyperthermophilic eubacterium Aquifex aeolicus, *J. Biol. Chem. 278*, 37909−37915.
41. DeLano, W. L. (2002) *PYMOL*, DeLano Scientific, San Carlos, CA.
42. Thompson, J. D., Higgins, D. G., and Gibson, T. J. (1994) CLUSTAL W: Improving the sensitivity of progressive multiple sequence alignment through sequence weighting, position-specific gap penalties and weight matrix choice, *Nucleic Acids Res. 22*, 4673−4680.

BI047848A